

# Addressing the Low Solubility of a Solid Electrolyte Interphase Stabilizer in an Electrolyte by Composite Battery Anode Design

Xiancheng Wang,<sup>1</sup> Lin Fu,<sup>1</sup> Renming Zhan, Lingyue Wang, Guocheng Li, Mintao Wan, Xing-Long Wu, Zhi Wei Seh, Li Wang, and Yongming Sun\*



Cite This: <https://dx.doi.org/10.1021/acsami.1c01571>



Read Online

ACCESS |



Metrics & More

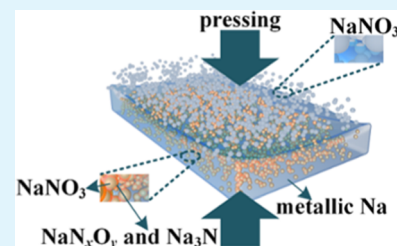


Article Recommendations



Supporting Information

**ABSTRACT:** Metallic sodium (Na) has been regarded as one of the most attractive anodes for Na-based rechargeable batteries due to its high specific capacity, low working potential, and high natural abundance. However, several important issues hinder the practical application of the metallic Na anode, including its high reactivity with electrolytes, uncontrolled dendrite growth, and poor processability. Metal nitrates are common electrolyte additives used to stabilize the solid electrolyte interphase (SEI) on Na anodes, though they typically suffer from poor solubility in electrolyte solvents. To address these issues, a Na/NaNO<sub>3</sub> composite foil electrode was fabricated through a mechanical kneading approach, which featured uniform embedment of NaNO<sub>3</sub> in a metallic Na matrix. During the battery cycling, NaNO<sub>3</sub> was reduced by metallic Na sustainably, which addressed the issue of low solubility of an SEI stabilizer. Due to the supplemental effect of NaNO<sub>3</sub>, a stable SEI with NaN<sub>x</sub>O<sub>y</sub> and Na<sub>3</sub>N species was produced, which allowed fast ion transport. As a result, stable electrochemical performance for 600 h was achieved for Na/NaNO<sub>3</sub>||Na/NaNO<sub>3</sub> symmetric cells at a current density of 0.5 mA cm<sup>-2</sup> and an areal capacity of 0.5 mAh cm<sup>-2</sup>. A Na/NaNO<sub>3</sub>||Na<sub>3</sub>V<sub>2</sub>(PO<sub>4</sub>)<sub>2</sub>O<sub>2</sub>F cell with active metallic Na of ~5 mAh cm<sup>-2</sup> at the anode showed stable cycling for 180 cycles. In contrast, a Na||Na<sub>3</sub>V<sub>2</sub>(PO<sub>4</sub>)<sub>2</sub>O<sub>2</sub>F cell only displayed less than 80 cycles under the same conditions. Moreover, the processability of the Na/NaNO<sub>3</sub> composite foil was also significantly improved due to the introduction of NaNO<sub>3</sub>, in contrast to the soft and sticky pure metallic Na. Mechanical kneading of soft alkali metals and their corresponding nitrates provides a new strategy for the utilization of anode stabilizers (besides direct addition into electrolytes) to improve their electrochemical performance.



**KEYWORDS:** metallic sodium, mechanical kneading, Na/NaNO<sub>3</sub> composite foil, NaN<sub>x</sub>O<sub>y</sub> and Na<sub>3</sub>N species, fast ion transport

## 1. INTRODUCTION

Sodium metal batteries (SMBs) with Na metal as anode materials have been considered as promising rechargeable batteries for grid energy storage and electric vehicles due to abundant Na resources, potentially low cost, reasonable working potential (−2.71 V vs standard hydrogen electrode), and high theoretical specific capacity (1166 mAh g<sup>-1</sup>) of the Na metal anode.<sup>1–3</sup> A metallic Na electrode is an essential component of SMBs but it encounters several serious issues that hinder the practical feasibility of SMBs. Due to the high reactivity of metallic Na, undesirable side reactions between metallic Na and the organic electrolyte take place continuously. Meanwhile, the solid electrolyte interphase (SEI) on the electrode surface breaks and repairs during the stripping/plating cycles of metallic Na, leading to the continuous consumption of the electrolyte and active metallic Na, as well as accumulation of thick SEI.<sup>4,5</sup> The above processes eventually cause large polarization, low Coulombic efficiency (CE), and fast failure of batteries.<sup>6,7</sup> Besides, due to the uncontrollable stripping/plating behavior of metallic Na, Na metal dendrites tend to grow, which may cause safety concerns of batteries.<sup>8,9</sup> Another big issue of metallic Na is its poor

processability due to its soft and sticky nature, making it more challenging for practical applications.<sup>10</sup>

Until now, several important publications have taken the directions of electrode surface coating,<sup>11,12</sup> construction of an artificial SEI film,<sup>13,14</sup> a Na metal composite,<sup>15,16</sup> solid electrolyte,<sup>17,18</sup> and optimization of electrolyte composition<sup>19,20</sup> to improve the electrochemical performance of Na metal electrodes. Significantly, through formation of a robust and stable SEI structure, electrolytes with nitrate and fluoride-based SEI stabilizers have imparted effective protection and good stability to Na metal electrodes.<sup>19,21,22</sup> With these SEI stabilizers dissolved in electrolytes, robust SEI forms through their reductive reaction with metallic Na, which helps to alleviate the side reactions between metallic Na and the organic electrolyte, homogenize Na<sup>+</sup> diffusion through the SEI and suppress dendrite growth.<sup>23,24</sup> Among these SEI stabilizers,

**Received:** January 24, 2021

**Accepted:** March 2, 2021

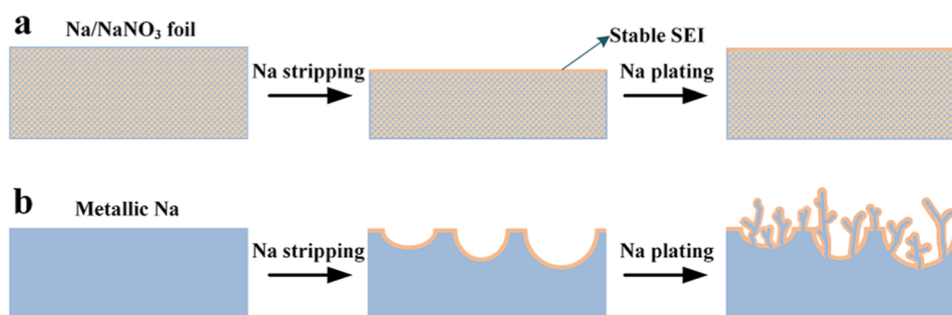


**Figure 1.** Schematic diagram of the Na stripping/plating behavior of the Na/NaNO<sub>3</sub> composite and pure metallic Na electrodes. With uniform NaNO<sub>3</sub> and its reductive species (NaN<sub>x</sub>O<sub>y</sub><sup>-</sup> and Na<sub>3</sub>N) implanted in the bulk of metallic Na, (a) stable SEI with fast Na<sup>+</sup> diffusion capability can be generated and uniform Na stripping and plating behavior can be realized, while (b) uneven SEI would form on the pure Na metal electrode, causing uneven Na stripping/plating behavior and even the growth of Na metal dendrites.

metal nitrates (e.g., LiNO<sub>3</sub>, NaNO<sub>3</sub>, and KNO<sub>3</sub>) show their unique advantage in the interphase structure with enhanced ionic conductivity by formation of N<sub>x</sub>O<sub>y</sub><sup>-</sup> and N<sup>3-</sup> species-rich SEI.<sup>25–27</sup> However, the practical application of these nitrate-based SEI stabilizers as electrolyte additives is limited by their solubility in the electrolyte solvents. Typically, they have very low solubility in carbonate-based solvents that are the most successful solvents for commercial electrolytes due to their high voltage window and good safety.<sup>28,29</sup> Therefore, it is highly desirable to explore a general approach to break the limit of low solubility of SEI stabilizers and realize their facile applications in batteries with various electrolytes, which is beneficial for realizing high-performance rechargeable alkali metal batteries and promote their practical applications.

Herein, using NaNO<sub>3</sub> for sodium metal batteries as an example, we directly introduced a SEI stabilizer (NaNO<sub>3</sub>, 15 wt % based on the mass of the entire electrode) into the bulk of a soft alkali metal (metallic Na) uniformly through a mechanical kneading approach and fabricated a composite Na/NaNO<sub>3</sub> foil electrode. In this electrode, the NaNO<sub>3</sub> was in situ reduced and was involved in the formation of a robust NaN<sub>x</sub>O<sub>y</sub> and Na<sub>3</sub>N species-rich SEI, which can homogenize Na<sup>+</sup> flow and accelerate their diffusion through the SEI due to enhanced ionic conductivity, and decrease the side reactions between the active metallic Na and electrolyte. Moreover, due to the uniform distribution of NaNO<sub>3</sub> and its reductive products within the bulk metallic Na, the processability of the as-fabricated Na/NaNO<sub>3</sub> composite foil was significantly improved. As expected, stable cycling of 600 h with low voltage polarization was achieved for the Na/NaNO<sub>3</sub> electrode in a symmetric cell configuration at 0.5 mA cm<sup>-2</sup> and 0.5 mAh cm<sup>-2</sup> in a carbonate-based electrolyte. Furthermore, a Na/NaNO<sub>3</sub>||Na<sub>3</sub>V<sub>2</sub>(PO<sub>4</sub>)<sub>2</sub>O<sub>2</sub>F (NVPOF) cell with a Na anode areal capacity loading of ~5 mAh cm<sup>-2</sup> sustained stable cycling for over 180 cycles, while the Na||NVPOF cell with the bare Na anode displayed fast capacity fade after 70 cycles.

## 2. EXPERIMENTAL SECTION

**2.1. Fabrication of the Na/NaNO<sub>3</sub> Composite Foil.** The Na/NaNO<sub>3</sub> composite foil was prepared through a simple mechanical kneading approach at room temperature in an Ar-filled glovebox (Mikrouna). NaNO<sub>3</sub> powder was first placed on the surface of a Na metal foil. The Na foil with NaNO<sub>3</sub> was repeatedly folded and calendered using a rolling machine until NaNO<sub>3</sub> was uniformly implanted within the metallic Na bulk. The mass contents of the NaNO<sub>3</sub> salts in the composite electrodes were fixed at 15 wt % based on the entire composite foil.

## 2.2. Preparation of Na<sub>3</sub>V<sub>2</sub>(PO<sub>4</sub>)<sub>2</sub>O<sub>2</sub>F (NVPOF) Electrodes.

NVPOF powder was prepared according to the previously reported method.<sup>30,31</sup> The slurry for NVPOF electrode fabrication contained a 70 wt % active material, 20 wt % conductive additive (carbon black), and 10 wt % binder (carboxymethylcellulose, CMC). After coating the slurry on the aluminum foil and drying in a vacuum oven at 60 °C, the NVPOF electrodes were fabricated. The average mass loading of the NVPOF electrodes was ~2.4 mg cm<sup>-2</sup>.

## 2.3. Preparation of Sulfurized Pyrolyzed Poly(acrylonitrile) (SPAN) Electrodes.

To fabricate SPAN, sulfur (S) and poly(acrylonitrile) (PAN) were mixed with a mass ratio of 1.75:1, sealed in a steel hydrothermal reactor (HTF-25-SS1, Anhui Kemi Machinery Technology Co., Ltd.) in an Ar atmosphere and treated at 350 °C for 10 h. A slurry approach was adopted to fabricate the SPAN electrode. The SPAN electrode contained an 80 wt % active material, a 10 wt % carbon black, and 10 wt % polyacrylic acid (PAA) binder. The average mass loading of SPAN electrodes was ~4.5 mg cm<sup>-2</sup>.

**2.4. Materials Characterization.** X-ray diffraction (XRD, PANalytical B.V.) was performed to identify the phase information of the Na/NaNO<sub>3</sub> composite foil. The surface states and compositions of the Na/NaNO<sub>3</sub> composite foil were characterized by X-ray photoelectron spectroscopy (XPS, AXIS-ULTRA DLD-600W). The morphology and structure of the electrodes were observed under a field emission scanning electron microscope (FESEM, Gemini SEM 300) equipped with an energy dispersive X-ray spectrum (EDX) analyzer.

**2.5. Electrochemical Measurements.** 2032 type coin cells were assembled for electrochemical measurements. Glass fiber (Whatman GF/D) was used as the separator and 1 M NaClO<sub>4</sub> in 1:1 ethylene carbonate (EC)/diethyl carbonate (DEC) with a 5wt% fluoroethylene carbonate (FEC) additive was used as the electrolyte. Electrochemical impedance spectrum (EIS), cyclic voltammetry (CV), and linear sweep voltammetry (LSV) measurements were conducted on a Biologic VMP3 electrochemical workstation. EIS was measured at the frequency range from 100 mHz to 100 kHz. CV was conducted at a voltage range from -0.2 to 0.2 V with a sweep rate of 1 mV s<sup>-1</sup>. Na/NaNO<sub>3</sub>||Na/NaNO<sub>3</sub> and Na||Na symmetric cells were assembled and tested by LSV, and the voltage range was from -0.13 to 0.13 V with the sweep rate of 1 mV s<sup>-1</sup>. Tafel curves and the exchange current density were plotted based on the LSV results. Galvanostatic cycling measurements were carried out on a Neware battery tester with a fixed current density and capacity for symmetric cells. The Na/NaNO<sub>3</sub>||NVPOF and Na||NVPOF cells were first cycled at 0.5C (1C = 130 mA g<sup>-1</sup>) for the initial 3 cycles and then at 5C at a voltage range from 2.0 to 4.3 V. Cells paired with the SPAN cathodes were activated at 20 mA g<sup>-1</sup> for the initial 5 cycles and then cycled at 200 mA g<sup>-1</sup> in the voltage range between 1.0 and 3.0 V.

## 3. RESULTS AND DISCUSSION

We highlight the importance of fast ionic transfer capability through SEI for Na metal electrodes, which could homogenize

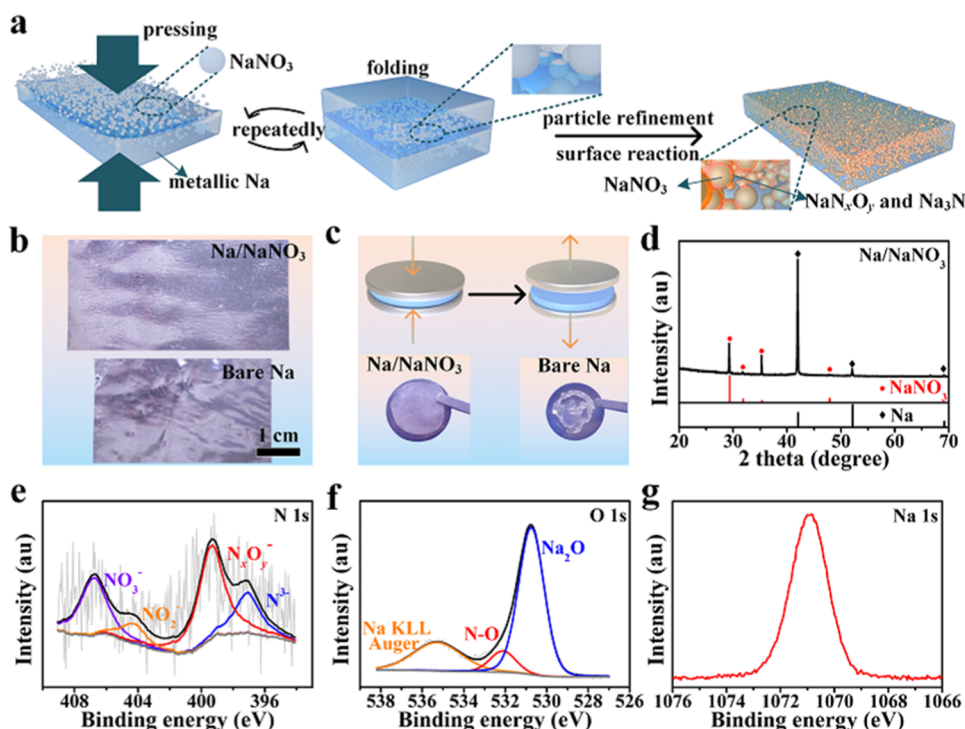


**Figure 2.** (a) Schematic diagram of the fabrication of the Na/NaNO<sub>3</sub> composite foil using a mechanical kneading approach. Repeated folding and calendaring operations are adopted to fabricate the Na/NaNO<sub>3</sub> composite foil. (b) Digital photos of the Na/NaNO<sub>3</sub> composite foil and the pure metallic Na foil with the same thickness of 400 μm and (c) after the release from an external mechanical pressure of 10 MPa in a coin cell. (d) XRD results of the Na/NaNO<sub>3</sub> composite foil, corresponding to NaNO<sub>3</sub> (JCPDS #36-1474) and pure metallic Na (JCPDS #22-0948). High-resolution XPS spectra of (e) N 1s, (f) O 1s, and (g) Na 1s for the Na/NaNO<sub>3</sub> composite foil.

the ion diffusion and improve the cycling stability. As illustrated in Figure 1a, with NaNO<sub>3</sub> as the SEI stabilizer, ionically conductive NaN<sub>x</sub>O<sub>y</sub> and Na<sub>3</sub>N species are produced through the reduction reaction by metallic Na and uniformly distributed over the entire electrode, enabling uniform Na<sup>+</sup> flow on the electrode surface and stable SEI, and eventually a prolonged cycle life of SMBs. In contrast, the inhomogeneous Na<sup>+</sup> flow through SEI would lead to an uncontrollable Na stripping and plating behavior, and Na dendrites with a high accessible area to the electrolyte would form. As a result, a thick SEI would accumulate quickly due to the severe side reactions between metallic Na and the electrolyte, leading to fast decay in battery performance and even safety concerns of SMBs.<sup>32</sup>

We fabricated a Na/NaNO<sub>3</sub> composite foil by a mechanical kneading approach. Utilizing the sticky property of metallic Na, NaNO<sub>3</sub> can be easily embedded into the bulk of metallic Na uniformly by repeated folding and calendaring cycles, as shown in Figure 2a. Note that during the mechanical kneading, large NaNO<sub>3</sub> particles break into small ones, which helps to realize the uniform distribution of NaNO<sub>3</sub>. Also, the mechanical kneading process enables a close contact between NaNO<sub>3</sub> and metallic Na, and the reduction reaction takes place spontaneously on their interphase, producing ionically conductive NaN<sub>x</sub>O<sub>y</sub> and Na<sub>3</sub>N species. Figure 2b shows a digital photo of the as-prepared Na/NaNO<sub>3</sub> (15 wt % NaNO<sub>3</sub>) composite foil with a thickness of 400 μm and size of 5.0 cm × 2.5 cm, which reveals a flat and smooth surface. In contrast, a rough surface is observed for the bare metallic Na with the same thickness due to the sticky property of metallic Na. Moreover, the composite shows much improved mechanical properties than the pure metallic Na, which is easy to cut

into regular pieces (Figure S1). This improved processability was further verified by the press and release experiment (Figure 2c). After the release from an external mechanical pressure of 10 MPa in a coin cell, the Na/NaNO<sub>3</sub> electrode well maintained its integrity and was easy to be separated from the stainless-steel clamps. On the contrary, the pure metallic Na was severely damaged and stuck on the stainless-steel clamps. Also, a thin and intact Na/NaNO<sub>3</sub> composite foil (~80 μm) was realized after calendaring operations (Figure S2a,b), while the bare metallic Na could not sustain the foil shape with a much larger thickness (~240 μm) due to its sticky nature (Figure S2c,d). The superior mechanical properties of the Na/NaNO<sub>3</sub> composite make it facile for future application in the electrode preparation and cell assembly processes.

The phase information of the Na/NaNO<sub>3</sub> composite foil was investigated by X-ray diffraction (XRD). As shown in Figure 2d, diffraction peaks at 2θ positions of 42.08, 52.18, and 69.18° were ascribed to metallic Na (JCPDS #22-0948), and peaks at 29.38, 31.86, and 35.36° arose from NaNO<sub>3</sub> (JCPDS #36-1474), indicating the coexistence of metallic Na and NaNO<sub>3</sub>. There was no observable phase information for NaN<sub>x</sub>O<sub>y</sub> and Na<sub>3</sub>N species according to the XRD results, probably due to their small size, amorphous structure, or/and small amount. The morphology characterization of the Na/NaNO<sub>3</sub> composite was carried out using a scanning electron microscope (SEM). As shown in Figure S3a, a flat and smooth surface was observed in the top-view SEM image of the Na/NaNO<sub>3</sub> composite foil in contrast to the rough and nonuniform surface of the pure metallic Na foil due to the soft and sticky properties (Figure S3b). The results of elemental mapping further verified the uniform composite of Na and NaNO<sub>3</sub> in the Na/NaNO<sub>3</sub> composite foil (Figure S4),

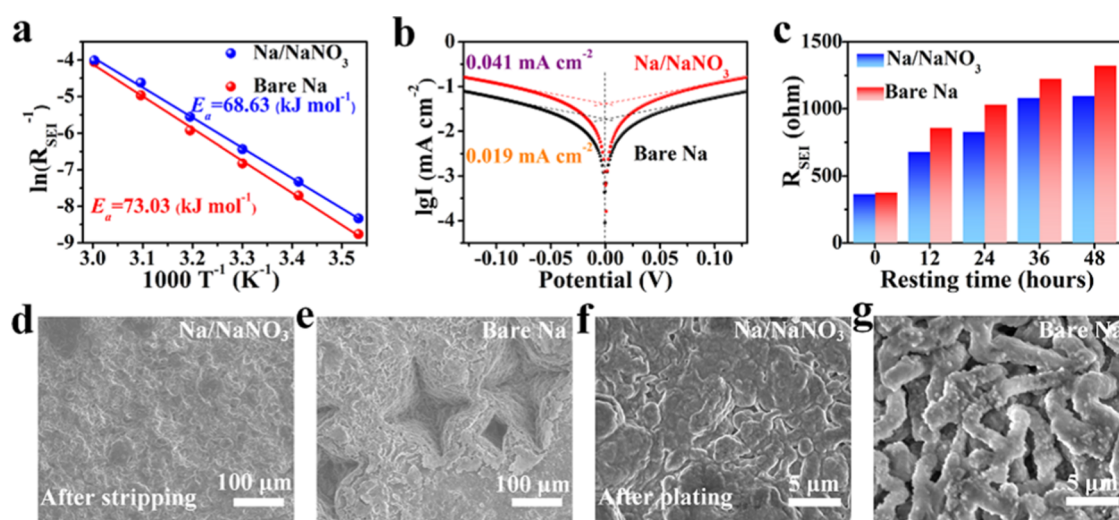


**Figure 3.** (a) Linearly fitted graph of the relationship between  $\ln(R_{\text{SEI}}^{-1})$  and  $T^{-1}$ , (b) Tafel curves and the calculated exchange current density of the Na/NaNO<sub>3</sub> and pure Na electrode from the linear sweep voltammetry tests and (c) comparison of fitted  $R_{\text{SEI}}$  values after different resting times for the Na/NaNO<sub>3</sub> and bare Na electrodes. Top-view SEM images of (d) Na/NaNO<sub>3</sub> composite and (e) pure metallic Na electrodes after stripping and (f, g) after plating at 1 mA cm<sup>-2</sup> and 3 mAh cm<sup>-2</sup>.  $R_{\text{SEI}}$  is the interface impedance between the electrode and electrolyte and  $E_a$  is the Na<sup>+</sup> diffusion energy barrier through the SEI. A smooth surface was observed for the Na/NaNO<sub>3</sub> electrode in contrast to the existence of large pits for the bare Na electrode after stripping.

which is beneficial for the formation of homogeneous SEI. To evaluate the specific capacity of metallic Na in the Na/NaNO<sub>3</sub> composite foil, Na ions were electrochemically extracted by galvanostatic charging of a Na/NaNO<sub>3</sub>||Na half cell to 1 V at 0.2 mA cm<sup>-2</sup> (Figure S5). The Na/NaNO<sub>3</sub> composite foil showed a high specific capacity of ~884.7 mAh g<sup>-1</sup> at the end of the metallic Na stripping process, maintaining the advantage of the high specific capacity of metallic Na.

X-ray photoelectron spectroscopy (XPS) was conducted to identify the surface composition of the Na/NaNO<sub>3</sub> composite foil. The high-resolution N 1s XPS spectrum shows the signal for NO<sub>3</sub><sup>-</sup>, indicating the existence of NaNO<sub>3</sub> in the Na/NaNO<sub>3</sub> composite (Figures 2e and S6a).<sup>33</sup> Besides, signals for NO<sub>2</sub><sup>-</sup>, N<sub>x</sub>O<sub>y</sub><sup>-</sup>, and N<sup>3-</sup> were also observed, corresponding to the reduction species of NaNO<sub>3</sub> by metallic Na.<sup>34,35</sup> The existence of N–O bonds and Na<sub>2</sub>O was verified in the Na/NaNO<sub>3</sub> composite foil according to the results of high-resolution O 1s spectra of the Na/NaNO<sub>3</sub> composite foil and NaNO<sub>3</sub>, further suggesting the coexistence of NaNO<sub>3</sub> and its reductive species (Figures 2f and S6b).<sup>36,37</sup> Compared with the results in high-resolution Na 1s of NaNO<sub>3</sub> powder (Figure S6c), the high-resolution Na 1s spectrum of the Na/NaNO<sub>3</sub> composite foil showed a larger binding energy than that of the pure metallic Na (Figure 2g). According to the results of the high-resolution spectra of N 1s and O 1s of the Na/NaNO<sub>3</sub> composite foil and Na 1s of the NaNO<sub>3</sub> powder, we could infer that the peaks in the high-resolution Na 1s spectrum of the Na/NaNO<sub>3</sub> composite foil correspond to the overlaps of metallic Na, NaNO<sub>3</sub>, and its reductive species. The composition of SEI is primarily dominated by the electrode and electrolyte components, which could regulate the deposition behavior of alkali metals.<sup>3,38</sup> The existence of Na<sub>n</sub>O<sub>y</sub> and Na<sub>3</sub>N species with good Na<sup>+</sup> conduction ability on the surface of the Na/NaNO<sub>3</sub> composite electrode could homogenize the Na<sup>+</sup> flow and accelerate their transfer through SEI. NaNO<sub>3</sub> in the Na/NaNO<sub>3</sub> composite foil would participate in the formation/repair of SEI during cycling and

help to construct a stable SEI that suppresses the side reactions between metallic Na and electrolyte.

To investigate the effect of NaNO<sub>3</sub> and its reduction species on the interface property of the composite Na/NaNO<sub>3</sub> electrode, the Na<sup>+</sup> diffusion energy barrier  $E_a$  through the SEI was calculated according to the electrochemical impedance spectrum (EIS) results. EIS of the Na/NaNO<sub>3</sub>||Na/NaNO<sub>3</sub> and Na||Na symmetric cells was performed at different temperatures (from 283 to 333 K) and the Nyquist points were fitted according to the equivalent circuit model in Figure S7 (Nyquist points after fitting are shown in Figure S8a,b).  $R_{\text{SEI}}$  corresponded to the interface impedance between the electrode and electrolyte (the values are shown in Table S1 and Figure S8c), whose relationships with  $E_a$  were described in the Arrhenius formula:  $R_{\text{SEI}}^{-1} = A \exp(-E_a/RT)$ .<sup>39</sup> According to the linear fitting results between  $\ln(R_{\text{SEI}}^{-1})$  and  $E_a$  shown in Figure 3a, the calculated value of  $E_a$  for the Na/NaNO<sub>3</sub> electrode was much smaller than that of the pure metallic Na (68.63 for the Na/NaNO<sub>3</sub> electrode vs 73.03 kJ mol<sup>-1</sup> for the pure metallic Na electrode), indicating the enhanced Na<sup>+</sup> diffusion through the SEI on the Na/NaNO<sub>3</sub> electrode. Tafel curves were further plotted according to the results of linear sweep voltammetry (LSV) measurements (Figure 3b).<sup>40,41</sup> The Na/NaNO<sub>3</sub> electrode exhibited a significantly increased exchange current density of 0.041 mA cm<sup>-2</sup> in comparison to 0.019 mA cm<sup>-2</sup> for the bare metallic Na, indicating faster ionic transfer kinetics for the SEI on the Na/NaNO<sub>3</sub> electrode.<sup>40,42</sup> Cyclic voltammetry (CV) measurement was further conducted to investigate the ion transfer kinetics of the Na/NaNO<sub>3</sub> electrode (Figure S9). The larger peak area and higher deposition current density of the Na/NaNO<sub>3</sub> electrode (1.5 mA cm<sup>-2</sup> compared with bare Na electrode of 1.0 mA cm<sup>-2</sup>) revealed the favorable SEI properties for Na deposition.<sup>39,43</sup>

The stability of the interface between the electrode and electrolyte was studied according to the EIS results of the Na/NaNO<sub>3</sub>||Na/NaNO<sub>3</sub> and Na||Na symmetric cells after different resting times. The Nyquist plots (Figure S10) were fitted according to the equivalent circuit model (Figure S7) and the

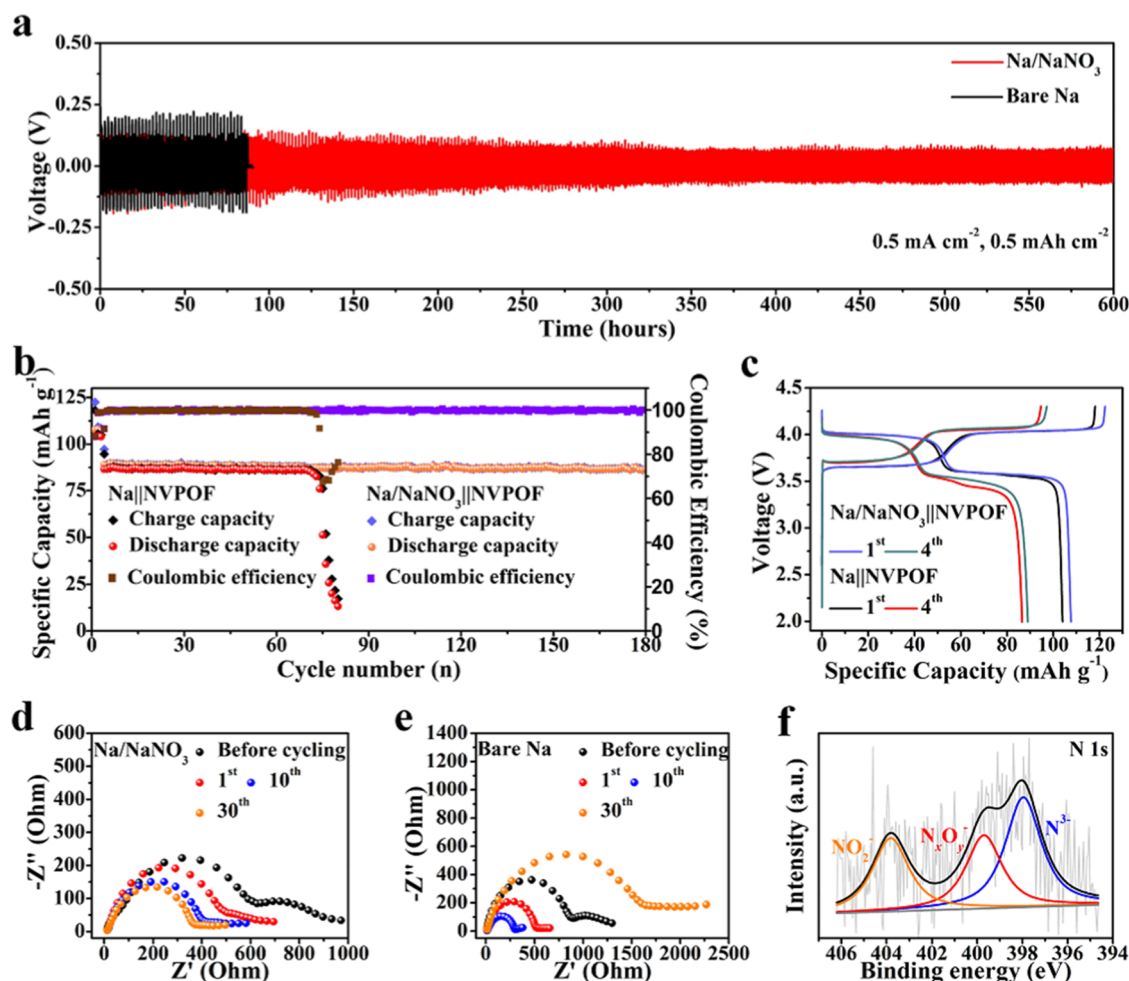


**Figure 4.** Electrochemical performance of the Na/NaNO<sub>3</sub> and metallic Na electrodes. (a) Voltage profiles of the Na/NaNO<sub>3</sub>||Na/NaNO<sub>3</sub> and Na||Na symmetric cells cycled at 0.5 mA cm<sup>-2</sup> and 0.5 mAh cm<sup>-2</sup>. (b) Cycling performance of Na/NaNO<sub>3</sub>||NVPOF and Na||NVPOF cells and (c) the corresponding charge/discharge profiles after the 1<sup>st</sup> and 4<sup>th</sup> cycles. The cells were cycled at 0.5C (1C = 130 mA g<sup>-1</sup>) for the initial 3 cycles followed by cycling at 2C at a voltage range from 2.0 to 4.3 V. (d, e) Nyquist plots of the Na/NaNO<sub>3</sub>||Na/NaNO<sub>3</sub> and Na||Na symmetric cells after different cycles and (f) high-resolution N 1s spectrum of the Na/NaNO<sub>3</sub> electrode after 50 cycles at 1 mA cm<sup>-2</sup> and 1 mAh cm<sup>-2</sup>.

values of  $R_{SEI}$  are shown in Table S2.  $R_{SEI}$  values after different resting times were compared for different electrodes (Figure 3c). The Na/NaNO<sub>3</sub> electrode showed a low interface impedance with a slight increase at the initial 24 h and stabilized after 36 h of resting ( $\sim 1081 \Omega$  after 36 h and  $1096 \Omega$  after 48 h of resting), while the pure metallic Na electrode exhibited continuously increased values of impedance during resting ( $\sim 1225 \Omega$  after 36 h and  $1322 \Omega$  after 48 h). This result suggests the stable interphase structure of the Na/NaNO<sub>3</sub> electrode and the suppressed side reactions between the electrode and electrolyte due to the existence and uniform distribution of NaNO<sub>3</sub>, NaN<sub>x</sub>O<sub>y</sub>, and Na<sub>3</sub>N species on the surface of the Na/NaNO<sub>3</sub> electrode.

The electrochemical Na stripping/plating behavior of the Na/NaNO<sub>3</sub> composite and pure metallic Na electrodes has been investigated. The SEM measurement was carried out for electrodes after a half stripping/plating cycle at 1 mA cm<sup>-2</sup> and 3 mAh cm<sup>-2</sup>, in a symmetric cell configuration. The Na/NaNO<sub>3</sub> composite electrode displayed a uniform and flat surface under the top-view SEM image (Figure 3d), indicating a uniform electrochemical stripping behavior due to the existence of the NaN<sub>x</sub>O<sub>y</sub> and Na<sub>3</sub>N species-rich SEI structure. In contrast, irregular pits with sizes ranging from  $\sim 50$  to 200

$\mu\text{m}$  were observed for the pure metallic Na electrode after Na stripping under SEM, indicating an inhomogeneous stripping behavior (Figure 3e). The deposits on the Na/NaNO<sub>3</sub> composite electrode after plating are densely packed, without the dendritic morphology (Figure 3f). The uniform stripping and dense plating behaviors of metallic Na could significantly prolong the lifespan of the Na metal anode.<sup>44,45</sup> As a comparison, mossy-like Na deposits or even Na dendrites were observed for the pure Na electrode after Na plating (Figure 3g). Such an inhomogeneous stripping/plating behavior for pure metallic Na would lead to the fast degradation of electrochemical performance during cycling.<sup>46,47</sup> The structures of the Na/NaNO<sub>3</sub> and pure Na electrodes after 10 cycles at 1 mA cm<sup>-2</sup> and 1 mAh cm<sup>-2</sup>, were also investigated (Figure S11a,b). Similar to the initial Na stripping/plating process, a flat and uniform surface morphology was also observed for the cycled Na/NaNO<sub>3</sub> electrode, further confirming the uniform Na stripping/plating behavior of the Na/NaNO<sub>3</sub> electrode, which will be beneficial for improving its cycling stability. The existence of the NaN<sub>x</sub>O<sub>y</sub> and Na<sub>3</sub>N species-rich SEI structure for the Na/NaNO<sub>3</sub> composite electrode imparted fast ionic transfer kinetics (Figures 3a,b and S9), enabling rapid and homogeneous Na<sup>+</sup>

flow through SEI. Thus, the uniform Na stripping/plating behavior and suppression of Na dendrites were achieved, which was essential for a long cycle life.

The galvanostatic charge/discharge measurement was carried out for the Na/NaNO<sub>3</sub> electrode. Significantly improved electrochemical reversibility was achieved for the Na/NaNO<sub>3</sub> electrode. Figure 4a shows the voltage profiles of the Na/NaNO<sub>3</sub>||Na/NaNO<sub>3</sub> and Na||Na symmetric cells cycled at 0.5 and 0.5 mAh cm<sup>-2</sup>. In comparison to the pure metallic Na electrode, the Na/NaNO<sub>3</sub> electrode showed a lower overpotential, more stable voltage curve, and significantly extended cycle lifetime. The voltage profiles remained stable for the Na/NaNO<sub>3</sub> electrode over 600 h, while the pure metallic Na electrode was short-circuited after 90 h, indicating improved cycling stability of the former. The voltage profiles of the Na/NaNO<sub>3</sub> electrode remained stable and the overpotential became smaller upon cycling, which may be ascribed to the stabilization process of the electrode with the introduction of NaNO<sub>3</sub>. When the current density and areal capacity increased to 1 mA cm<sup>-2</sup> and 1 mAh cm<sup>-2</sup>, respectively, the Na/NaNO<sub>3</sub> electrode showed a low average overpotential and greatly improved cycling stability over 500 h (Figure S12). Stable cycling was also achieved for the Na/NaNO<sub>3</sub> electrode at 1 mA cm<sup>-2</sup> with a fixed areal capacity of 3 mAh cm<sup>-2</sup> (400 h in Figure S13), and 3 mA cm<sup>-2</sup> with a fixed areal capacity of 2 mAh cm<sup>-2</sup> (150 h in Figure S14).

The electrochemical performance of the Na/NaNO<sub>3</sub> composite foil electrode was further investigated in cells with the NVPOF cathode. The active materials' loading was ~2.4 mg cm<sup>-2</sup> for the NVPOF cathode and the areal capacity loading was ~5 mAh cm<sup>-2</sup> for the Na/NaNO<sub>3</sub> anode. Figure 4b showed the capacity–cycle number plots of the Na/NaNO<sub>3</sub>||NVPOF and Na||NVPOF cells (0.5C for the initial 3 cycles and 2C for the following cycles, 1C = 130 mA g<sup>-1</sup>). The Na/NaNO<sub>3</sub>||NVPOF cells sustained stable cycling for 180 cycles, while the Na||NVPOF cells exhibited fast capacity fading after 75 cycles, indicating the much improved electrochemical reversibility of the Na/NaNO<sub>3</sub> electrode due to the introduction of NaNO<sub>3</sub>. Charge/discharge curves revealed the steady charge/discharge plateau and reduced polarization for the Na/NaNO<sub>3</sub>||NVPOF cell in comparison to the Na||NVPOF cell (Figures 4c and S15), further confirming the improved electrochemical performance benefiting from the NaN<sub>x</sub>O<sub>y</sub> and Na<sub>3</sub>N species-rich SEI with fast charge transfer kinetics. To demonstrate the application of the Na/NaNO<sub>3</sub> electrode in cells with high-capacity battery cathodes such as sulfur-based cathodes, Na/NaNO<sub>3</sub>||SPAN cells were assembled and measured (Figure S16). They displayed high reversible capacities (~370 mAh g<sup>-1</sup> based on the mass of SPAN), good capacity retention of 64% (cycling at 200 mA g<sup>-1</sup>) for 100 cycles with reduced polarization (Figure S17), further revealing the improved electrochemical performance, and potential application of the Na/NaNO<sub>3</sub> composite foil.

EIS measurement of the Na/NaNO<sub>3</sub>||Na/NaNO<sub>3</sub> cell after different cycles (cycling at 1 mA cm<sup>-2</sup>, 1 mAh cm<sup>-2</sup>) was carried out to verify the interface stability of the Na/NaNO<sub>3</sub> electrode (Figure 4d,e). The Na/NaNO<sub>3</sub> electrode showed a much lower interface impedance (~620 Ω) compared to the bare Na electrode (~900 Ω) before cycling, suggesting enhanced ionic conductivity due to the formation of the NaN<sub>x</sub>O<sub>y</sub> and Na<sub>3</sub>N species-containing electrode and interphase structure. The interface impedance of the Na/NaNO<sub>3</sub> electrode was ~500 Ω after the 1st cycle, which decreased

to ~370 Ω after the 30th cycle, indicating the formation of a stable SEI during the stripping/plating cycling of metallic Na. The interface impedance of the bare metallic Na electrode was ~520 Ω after the first cycle, which was slightly lower than that before cycling due to the break of the native oxide layer and the dendrite growth as observed in SEM (Figure 3g). Along with the growth of mossy and dendrite-like metallic Na, the interface impedance of the metallic Na electrode continued decreasing on cycling and the value was reduced to ~300 Ω after 10 cycles. Continuous accumulation of SEI and the consumption of the electrolyte during the repeated side reactions between metallic Na and the electrolyte eventually led to a large impedance of the pure metallic Na electrode after many cycles, which hindered charge transfer.<sup>48</sup> Thus, the interface impedance of the metallic Na electrode after 30 cycles increased to ~1650 Ω, suggesting poor interphase stability and inferior cycling stability of the pure metallic Na electrode.<sup>49</sup>

To further understand the enhanced performance of the Na/NaNO<sub>3</sub> electrode, the interphase composition after Na stripping/plating cycles was further investigated using XPS. The results of high-resolution N 1s and O 1s spectra showed the existence of NO<sub>2</sub><sup>-</sup>, N<sub>x</sub>O<sub>y</sub><sup>-</sup>, N<sup>3+</sup>, and Na<sub>2</sub>O components on the surface of the Na/NaNO<sub>3</sub> electrode after 50 cycles at 1 mA cm<sup>-2</sup> and 1 mAh cm<sup>-2</sup>,<sup>34,35</sup> indicating the long-term stability and the effect of the N-containing species during the repeated cycling processes (Figures 4f and S18a). Besides the N-containing species, NaCl (Cl 2p in Figure S18b),<sup>13</sup> NaF (F 1s in Figure S18c),<sup>27</sup> and Na<sub>2</sub>CO<sub>3</sub> and –C–O– (O 1s and C 1s in Figure S18d) were also observed,<sup>50</sup> corresponding to the decomposition products of electrolyte components of NaClO<sub>4</sub>, fluoroethylene carbonate (FEC), and other organic solvents, respectively. Besides, the Na signal in the high-resolution Na 1s spectrum (Figure S18e) arises from metallic Na and its oxidation state. The XPS results revealed the good stability of the NaN<sub>x</sub>O<sub>y</sub> and Na<sub>3</sub>N species-containing SEI on the electrode surface due to the supplemental effect of NaNO<sub>3</sub> that stabilized the interphase structure during cycling, which played an important role in improving the electrochemical performance of the composite anode.

#### 4. CONCLUSIONS

In conclusion, a Na/NaNO<sub>3</sub> composite battery anode was designed and fabricated by a mechanical kneading approach at room temperature. NaNO<sub>3</sub> was uniformly embedded into the bulk of metallic Na and partially reduced into NaN<sub>x</sub>O<sub>y</sub> and Na<sub>3</sub>N species, leading to good stability and Na<sup>+</sup> conductivity of the electrode. Moreover, the remaining NaNO<sub>3</sub> worked as a SEI stabilizer, which enabled the stable battery anode for long-term cycling. Such a method addresses the problem of poor solubility of many SEI stabilizers in electrolytes (e.g., nitrates in carbonate-based electrolyte) and expands their applications in different battery systems, which provides a new strategy for the use of SEI stabilizers to improve the electrochemical performance of the Na metal electrode. As expected, a stable Na stripping/plating behavior, a low overpotential, and stable interface impedance were obtained for the Na/NaNO<sub>3</sub> composite battery electrode. This facile strategy can potentially be extended to other alkali metal anodes to enhance their reversibility for next-generation energy storage devices.

## ■ ASSOCIATED CONTENT

### SI Supporting Information

The Supporting Information is available free of charge at <https://pubs.acs.org/doi/10.1021/acsami.1c01571>.

Additional digital and SEM images; additional XPS results; additional CVs and Nyquist plots; additional Tables for the fitting results of the Nyquist plots; and additional voltage profiles, cycle performance, and voltage curves (PDF)

## ■ AUTHOR INFORMATION

### Corresponding Author

**Yongming Sun** – Wuhan National Laboratory for Optoelectronics, Huazhong University of Science and Technology, Wuhan 430074, China; [orcid.org/0000-0001-8528-525X](https://orcid.org/0000-0001-8528-525X); Email: [yongmingsun@hust.edu.cn](mailto:yongmingsun@hust.edu.cn)

### Authors

**Xiancheng Wang** – Wuhan National Laboratory for Optoelectronics, Huazhong University of Science and Technology, Wuhan 430074, China

**Lin Fu** – Wuhan National Laboratory for Optoelectronics, Huazhong University of Science and Technology, Wuhan 430074, China; [orcid.org/0000-0001-6834-2881](https://orcid.org/0000-0001-6834-2881)

**Renming Zhan** – Wuhan National Laboratory for Optoelectronics, Huazhong University of Science and Technology, Wuhan 430074, China

**Lingyue Wang** – Wuhan National Laboratory for Optoelectronics, Huazhong University of Science and Technology, Wuhan 430074, China

**Guocheng Li** – Wuhan National Laboratory for Optoelectronics, Huazhong University of Science and Technology, Wuhan 430074, China

**Mintao Wan** – Wuhan National Laboratory for Optoelectronics, Huazhong University of Science and Technology, Wuhan 430074, China

**Xing-Long Wu** – MOE Key Laboratory for UV Light-Emitting Materials and Technology, and Faculty of Chemistry, Northeast Normal University, Changchun, Jilin 130024, China; [orcid.org/0000-0003-1069-9145](https://orcid.org/0000-0003-1069-9145)

**Zhi Wei Seh** – Institute of Materials Research and Engineering, Agency for Science, Technology and Research (A\*STAR), Singapore 138634, Singapore; [orcid.org/0000-0003-0953-567X](https://orcid.org/0000-0003-0953-567X)

**Li Wang** – Institute of Nuclear and New Energy Technology, Tsinghua University, Beijing 100084, China

Complete contact information is available at: <https://pubs.acs.org/10.1021/acsami.1c01571>

### Author Contributions

<sup>1</sup>X.W. and L.F. contributed equally to this work.

### Notes

The authors declare no competing financial interest.

## ■ ACKNOWLEDGMENTS

The authors would like to thank the support by the National Natural Science Foundation of China (No. 520721137, 51802105). Z.W.S. acknowledges the support of the Singapore National Research Foundation (NRF-NRFF2017-04). The authors would like to thank the Analytical and Testing Center of the Huazhong University of Science and Technology and Wuhan National Laboratory for Optoelectronics of Huazhong

University of Science and Technology for providing the facilities to conduct the characterization. X.W. would like to thank Yuanfang Zheng for the schematic diagram design. The authors would like to thank Dr. Qingwu Huang for his help on the analyses of XPS results.

## ■ REFERENCES

- (1) Lee, B.; Paek, E.; Mitlin, D.; Lee, S. W. Sodium Metal Anodes: Emerging Solutions to Dendrite Growth. *Chem. Rev.* **2019**, *119*, 5416–5460.
- (2) Fu, L.; Shang, C.; Ma, J.; Zhang, C.; Zang, X.; Chai, J.; Li, J.; Cui, G. Cu<sub>2</sub>GeS<sub>3</sub> Derived Ultrafine Nanoparticles as High-Performance Anode for Sodium Ion Battery. *Sci. China Mater.* **2018**, *61*, 1177–1184.
- (3) Sun, B.; Xiong, P.; Maitra, U.; Langsdorf, D.; Yan, K.; Wang, C.; Janek, J.; Schroder, D.; Wang, G. Design Strategies to Enable the Efficient Use of Sodium Metal Anodes in High-Energy Batteries. *Adv. Mater.* **2020**, *32*, No. 1903891.
- (4) Bao, C.; Wang, B.; Liu, P.; Wu, H.; Zhou, Y.; Wang, D.; Liu, H.; Dou, S. Solid Electrolyte Interphases on Sodium Metal Anodes. *Adv. Funct. Mater.* **2020**, *30*, No. 2004891.
- (5) Wu, W.; Hou, S.; Zhang, C.; Zhang, L. A Dendrite-Free Na-Na<sub>2</sub>S-Carbon Hybrid toward a Highly Stable and Superior Sodium Metal Anode. *ACS Appl. Mater. Interfaces* **2020**, *12*, 27300–27306.
- (6) Cui, J.; Wang, A.; Li, G.; Wang, D.; Shu, D.; Dong, A.; Zhu, G.; Luo, J.; Sun, B. Composite Sodium Metal Anodes for Practical Applications. *J. Mater. Chem. A* **2020**, *8*, 15399–15416.
- (7) Tang, S.; Zhang, Y. Y.; Zhang, X. G.; Li, J. T.; Wang, X. Y.; Yan, J. W.; Wu, D. Y.; Zheng, M. S.; Dong, Q. F.; Mao, B. W. Stable Na Plating and Stripping Electrochemistry Promoted by In Situ Construction of an Alloy-Based Sodiophilic Interphase. *Adv. Mater.* **2019**, *31*, No. 1807495.
- (8) Hu, X.; Joo, P. H.; Wang, H.; Matios, E.; Wang, C.; Luo, J.; Lu, X.; Yang, K.; Li, W. Nip the Sodium Dendrites in the Bud on Planar Doped Graphene in Liquid/Gel Electrolytes. *Adv. Funct. Mater.* **2019**, *29*, No. 1807974.
- (9) Fan, L.; Li, X. Recent Advances in Effective Protection of Sodium Metal Anode. *Nano Energy* **2018**, *53*, 630–642.
- (10) Wang, A.; Hu, X.; Tang, H.; Zhang, C.; Liu, S.; Yang, Y. W.; Yang, Q. H.; Luo, J. Processable and Moldable Sodium-Metal Anodes. *Angew. Chem., Int. Ed.* **2017**, *56*, 11921–11926.
- (11) Luo, W.; Lin, C.-F.; Zhao, O.; Noked, M.; Zhang, Y.; Rubloff, G. W.; Hu, L. Ultrathin Surface Coating Enables the Stable Sodium Metal Anode. *Adv. Energy Mater.* **2017**, *7*, No. 1601526.
- (12) Wang, H.; Liang, J.; Wu, Y.; Kang, T.; Shen, D.; Tong, Z.; Yang, R.; Jiang, Y.; Wu, D.; Li, X.; Lee, C. S. Porous BN Nanofibers Enable Long-Cycling Life Sodium Metal Batteries. *Small* **2020**, *16*, No. 2002671.
- (13) Zheng, X.; Fu, H.; Hu, C.; Xu, H.; Huang, Y.; Wen, J.; Sun, H.; Luo, W.; Huang, Y. Toward a Stable Sodium Metal Anode in Carbonate Electrolyte: A Compact, Inorganic Alloy Interface. *J. Phys. Chem. Lett.* **2019**, *10*, 707–714.
- (14) Kumar, V.; Eng, A. Y. S.; Wang, Y.; Nguyen, D.-T.; Ng, M.-F.; Seh, Z. W. An Artificial Metal-Alloy Interphase for High-rate and Long-life Sodium-sulfur Batteries. *Energy Storage Mater.* **2020**, *29*, 1–8.
- (15) Yoon, H. J.; Kim, N. R.; Jin, H.-J.; Yun, Y. S. Macroporous Catalytic Carbon Nanotemplates for Sodium Metal Anodes. *Adv. Energy Mater.* **2018**, *8*, No. 1701261.
- (16) Sun, Q.; Zhai, W.; Hou, G.; Feng, J.; Zhang, L.; Si, P.; Guo, S.; Ci, L. In Situ Synthesis of a Lithiophilic Ag-Nanoparticles-Decorated 3D Porous Carbon Framework toward Dendrite-Free Lithium Metal Anodes. *ACS Sustainable Chem. Eng.* **2018**, *6*, 15219–15227.
- (17) Zheng, Y.; Pan, Q.; Clites, M.; Byles, B. W.; Pomerantseva, E.; Li, C. Y. High-Capacity All-Solid-State Sodium Metal Battery with Hybrid Polymer Electrolytes. *Adv. Energy Mater.* **2018**, *8*, No. 1801885.

- (18) Fu, H.; Yin, Q.; Huang, Y.; Sun, H.; Chen, Y.; Zhang, R.; Yu, Q.; Gu, L.; Duan, J.; Luo, W. Reducing Interfacial Resistance by Na-SiO<sub>2</sub> Composite Anode for NASICON-Based Solid-State Sodium Battery. *ACS Mater. Lett.* **2020**, *2*, 127–132.
- (19) Seh, Z. W.; Sun, J.; Sun, Y.; Cui, Y. A Highly Reversible Room-Temperature Sodium Metal Anode. *ACS Cent. Sci.* **2015**, *1*, 449–455.
- (20) Lee, Y.; Lee, J.; Lee, J.; Kim, K.; Cha, A.; Kang, S.; Wi, T.; Kang, S. J.; Lee, H. W.; Choi, N. S. Fluoroethylene Carbonate-Based Electrolyte with 1 M Sodium Bis(fluorosulfonyl)imide Enables High-Performance Sodium Metal Electrodes. *ACS Appl. Mater. Interfaces* **2018**, *10*, 15270–15280.
- (21) Shi, Q.; Zhong, Y.; Wu, M.; Wang, H.; Wang, H. High-Performance Sodium Metal Anodes Enabled by a Bifunctional Potassium Salt. *Angew. Chem., Int. Ed.* **2018**, *57*, 9069–9072.
- (22) Shi, P.; Zhang, L.; Xiang, H.; Liang, X.; Sun, Y.; Xu, W. Lithium Difluorophosphate as a Dendrite-Suppressing Additive for Lithium Metal Batteries. *ACS Appl. Mater. Interfaces* **2018**, *10*, 22201–22209.
- (23) Fang, W.; Jiang, H.; Zheng, Y.; Zheng, H.; Liang, X.; Sun, Y.; Chen, C.; Xiang, H. A Bilayer Interface Formed in High Concentration Electrolyte with SbF<sub>3</sub> Additive for Long-Cycle and High-Rate Sodium Metal Battery. *J. Power Sources* **2020**, *455*, No. 227956.
- (24) Wang, S.; Cai, W.; Sun, Z.; Huang, F.; Jie, Y.; Liu, Y.; Chen, Y.; Peng, B.; Cao, R.; Zhang, G.; Jiao, S. Stable Cycling of Na metal Anodes in a Carbonate Electrolyte. *Chem. Commun.* **2019**, *55*, 14375–14378.
- (25) Guo, J.; Wen, Z.; Wu, M.; Jin, J.; Liu, Y. Vinylene Carbonate–LiNO<sub>3</sub>: A Hybrid Additive in Carbonic Ester Electrolytes for SEI Modification on Li Metal Anode. *Electrochem. Commun.* **2015**, *51*, 59–63.
- (26) Jia, W.; Fan, C.; Wang, L.; Wang, Q.; Zhao, M.; Zhou, A.; Li, J. Extremely Accessible Potassium Nitrate (KNO<sub>3</sub>) as the Highly Efficient Electrolyte Additive in Lithium Battery. *ACS Appl. Mater. Interfaces* **2016**, *8*, 15399–15405.
- (27) Yan, C.; Yao, Y. X.; Chen, X.; Cheng, X. B.; Zhang, X. Q.; Huang, J. Q.; Zhang, Q. Lithium Nitrate Solvation Chemistry in Carbonate Electrolyte Sustains High-Voltage Lithium Metal Batteries. *Angew. Chem., Int. Ed.* **2018**, *57*, 14055–14059.
- (28) Liu, Y.; Lin, D.; Li, Y.; Chen, G.; Pei, A.; Nix, O.; Li, Y.; Cui, Y. Solubility-mediated Sustained Release Enabling Nitrate Additive in Carbonate Electrolytes for Stable Lithium Metal Anode. *Nat. Commun.* **2018**, *9*, No. 3656.
- (29) Shi, Q.; Zhong, Y.; Wu, M.; Wang, H.; Wang, H. High-capacity Rechargeable Batteries Based on Deeply Cyclable Lithium Metal Anodes. *Proc. Natl. Acad. Sci. U.S.A.* **2018**, *115*, 5676–5680.
- (30) Guo, J. Z.; Wang, P. F.; Wu, X. L.; Zhang, X. H.; Yan, Q.; Chen, H.; Zhang, J. P.; Guo, Y. G. High-Energy/Power and Low-Temperature Cathode for Sodium-Ion Batteries: In Situ XRD Study and Superior Full-Cell Performance. *Adv. Mater.* **2017**, *29*, No. 1701968.
- (31) Guo, J.-Z.; Yang, Y.; Liu, D.-S.; Wu, X.-L.; Hou, B.-H.; Pang, W.-L.; Huang, K.-C.; Zhang, J.-P.; Su, Z.-M. A Practicable Li/Na-Ion Hybrid Full Battery Assembled by a High-Voltage Cathode and Commercial Graphite Anode: Superior Energy Storage Performance and Working Mechanism. *Adv. Energy Mater.* **2018**, *8*, No. 1702504.
- (32) Rakov, D. A.; Chen, F.; Ferdousi, S. A.; Li, H.; Pathirana, T.; Simonov, A. N.; Howlett, P. C.; Atkin, R.; Forsyth, M. Engineering High-energy-density Sodium Battery Anodes for Improved Cycling with Superconcentrated Ionic-liquid Electrolytes. *Nat. Mater.* **2020**, *19*, 1096–1101.
- (33) Baltrusaitis, J.; Jayaweera, P. M.; Grassian, V. H. XPS Study of Nitrogen Dioxide Adsorption on Metal Oxide Particle Surfaces under Different Environmental Conditions. *Phys. Chem. Chem. Phys.* **2009**, *11*, 8295–8305.
- (34) Wang, X.; Wang, H.; Liu, M.; Li, W. In-Plane Lithium Growth Enabled by Artificial Nitrate-Rich Layer: Fast Deposition Kinetics and Desolvation/Adsorption Mechanism. *Small* **2020**, *16*, No. 2000769.
- (35) Sahalie, N. A.; Assegie, A. A.; Su, W.-N.; Wondimkun, Z. T.; Jote, B. A.; Thirumalraj, B.; Huang, C.-J.; Yang, Y.-W.; Hwang, B.-J. Effect of Bifunctional Additive Potassium Nitrate on Performance of Anode Free Lithium Metal Battery in Carbonate Electrolyte. *J. Power Sources* **2019**, *437*, No. 226912.
- (36) Zhong, Y.; Xie, Y.; Hwang, S.; Wang, Q.; Cha, J. J.; Su, D.; Wang, H. A Highly Efficient All-Solid-State Lithium/Electrolyte Interface Induced by an Energetic Reaction. *Angew. Chem., Int. Ed.* **2020**, *59*, 14003–14008.
- (37) Qi, W.; Ben, L.; Yu, H.; Zhan, Y.; Zhao, W.; Huang, X. Improving the Electrochemical Cycling Performance of Anode Materials via Facile in Situ Surface Deposition of a Solid Electrolyte Layer. *J. Power Sources* **2019**, *424*, 150–157.
- (38) Lin, D.; Liu, Y.; Cui, Y. Reviving the Lithium Metal Anode for High-energy Batteries. *Nat. Nanotechnol.* **2017**, *12*, 194–206.
- (39) Ouyang, Y.; Guo, Y.; Li, D.; Wei, Y.; Zhai, T.; Li, H. Single Additive with Dual Functional-Ions for Stabilizing Lithium Anodes. *ACS Appl. Mater. Interfaces* **2019**, *11*, 11360–11368.
- (40) Lin, Y.; Wen, Z.; Yang, C.; Zhang, P.; Zhao, J. Strengthening Dendrite Suppression in Lithium Metal Anode by In-Situ Construction of Li–Zn alloy layer. *Electrochem. Commun.* **2019**, *108*, No. 106565.
- (41) Meng, J.; Chu, F.; Hu, J.; Li, C. Liquid Polydimethylsiloxane Grafting to Enable Dendrite-Free Li Plating for Highly Reversible Li-Metal Batteries. *Adv. Funct. Mater.* **2019**, *29*, No. 1902220.
- (42) Liang, X.; Pang, Q.; Kochetkov, I. R.; Sempere, M. S.; Huang, H.; Sun, X.; Nazar, L. F. A Facile Surface Chemistry Route to a Stabilized Lithium Metal Anode. *Nat. Energy* **2017**, *2*, No. 17119.
- (43) Zhang, Q.; Luan, J.; Huang, X.; Wang, Q.; Sun, D.; Tang, Y.; Ji, X.; Wang, H. Revealing the Role of Crystal Orientation of Protective Layers for Stable Zinc Anode. *Nat. Commun.* **2020**, *11*, No. 3961.
- (44) Tu, Z.; Choudhury, S.; Zachman, M. J.; Wei, S.; Zhang, K.; Kourkoutis, L. F.; Archer, L. A. Fast Ion Transport at Solid–Solid Interfaces in Hybrid Battery Anodes. *Nat. Energy* **2018**, *3*, 310–316.
- (45) Zheng, X.; Yang, W.; Wang, Z.; Huang, L.; Geng, S.; Wen, J.; Luo, W.; Huang, Y. Embedding a Percolated Dual-Conductive Skeleton with High Sodiophilicity Toward Stable Sodium Metal Anodes. *Nano Energy* **2020**, *69*, No. 104387.
- (46) Wan, M.; Kang, S.; Wang, L.; Lee, H. W.; Zheng, G. W.; Cui, Y.; Sun, Y. Mechanical Rolling Formation of Interpenetrated Lithium Metal/Lithium Tin Alloy Foil for Ultrahigh-Rate Battery Anode. *Nat. Commun.* **2020**, *11*, No. 829.
- (47) Hou, Z.; Wang, W.; Chen, Q.; Yu, Y.; Zhao, X.; Tang, M.; Zheng, Y.; Quan, Z. Hybrid Protective Layer for Stable Sodium Metal Anodes at High Utilization. *ACS Appl. Mater. Interfaces* **2019**, *11*, 37693–37700.
- (48) Liu, H.; Cheng, X.; Zhang, R.; Shi, P.; Shen, X.; Chen, X.; Li, T.; Huang, J.; Zhang, Q. Mesoporous Graphene Hosts for Dendrite-Free Lithium Metal Anode in Working Rechargeable Batteries. *Trans. Tianjin Univ.* **2020**, *26*, 127–134.
- (49) Wang, H.; Lin, D.; Liu, Y.; Li, Y.; Cui, Y. Ultrahigh-Current Density Anodes with Interconnected Li Metal Reservoir through Overlithiation of Mesoporous AlF<sub>3</sub> Framework. *Sci. Adv.* **2017**, *3*, No. e1701301.
- (50) Brown, Z. L.; Heiskanen, S.; Lucht, B. L. Using Triethyl Phosphate to Increase the Solubility of LiNO<sub>3</sub> in Carbonate Electrolytes for Improving the Performance of the Lithium Metal Anode. *J. Electrochem. Soc.* **2019**, *166*, A2523–A2527.